STRUCTURAL SCIENCE
CRYSTAL ENGINEERING
MATERIALS

ISSN: 2052-5206
journals.iucr.org/b

Exploring new belousovite-related zinc and cadmium alkali sulfate halides: synthesis and structural variability

Artem S. Borisov, Oleg I. Siidra, Dmitri O. Charkin, Karim A. Zagidullin, Ruslan K. Burshtynovich and Natalia S. Vlasenko

Acta Cryst. (2022). B**78**, 499–509

Acta Cryst B
STRUCTURAL SCIENCE
CRYSTAL ENGINEERING
MATERIALS
ISSN 2052-5206

Exploring new belousovite-related zinc and cadmium alkali sulfate halides: synthesis and structural variability

Artem S. Borisov,[a,b] Oleg I. Siidra,[a,c]* Dmitri O. Charkin,[d] Karim A. Zagidullin,[d] Ruslan K. Burshtynovich[d] and Natalia S. Vlasenko[e]

[a]Department of Crystallography, St. Petersburg State University, University emb. 7/9, St. Petersburg, 199034, Russian Federation, [b]Institute of Silicate Chemistry, Russian Academy of Sciences, Adm. Makarova emb. 2, St. Petersburg, 199034, Russian Federation, [c]Kola Science Center, Russian Academy of Sciences, Apatity, Murmansk Region 184200, Russian Federation, [d]Department of Inorganic Chemistry, Faculty of Chemistry, Moscow State University, Leninskie Gory 1-3, Moscow, 119991, Russian Federation, and [e]Geomodel Resource Center, St. Petersburg State University, University emb. 7/9, St. Petersburg, 199034, Russian Federation. *Correspondence e-mail: o.siidra@spbu.ru

Received 2 March 2022
Accepted 29 March 2022

Edited by O. V. Yakubovich, Moscow State University, Russian Federation

Keywords: sulfates; halides; belousovite; morphotropism; inorganic synthesis.

Supporting information: this article has supporting information at journals.iucr.org/b

Fourteen new belousovite-related compounds, AZn(TO$_4$)X (A = K, Rb, Cs, Tl, NH$_4$; T = S, Se; X = Cl, Br, I) have been prepared via melt and evaporation techniques by reacting AX and ZnTO$_4$ either at high temperatures or in hot aqueous solutions. They adopt the layered structure of the belousovite archetype, and constitute a morphotropic series. The apophyllite-type layers in these structures undergo different corrugations, most pronounced in the case of CsZn(SO$_4$)I. In addition, during the study two species unrelated to belousovite, namely Na$_4$Zn(SO$_4$)$_2$Cl$_2$ and Cs$_2$Cd$_3$(SO$_4$)$_4$, were found with framework crystal structures having different topology and belonging to new structure types.

1. Introduction

Anhydrous sulfate halides of transition metals exhibit a broad range of compositions, structures and properties, and attract increasing interest due to their prominent contributions in mineralogy (Vergasova & Filatov, 2016). In materials chemistry, most attention is paid to sulfate fluorides (*e.g.* Ati *et al.*, 2011; Reynaud *et al.*, 2012; Sun *et al.*, 2016). Synthetic derivatives of other halogens, namely Cl, Br and I, are rare and have been addressed mainly among compounds of copper due to their attractive magnetic properties (Hälg *et al.*, 2014; Kikuchi *et al.*, 2017; Soldatov *et al.*, 2018; Fujihala *et al.*, 2020*a*,*b*). For other elements, such compounds received less attention; particularly for zinc, these were addressed in a couple of contributions only (Bosson, 1973, 1976).

Recently, we have identified a new mineral species belousovite KZn(SO$_4$)Cl (Siidra *et al.*, 2018*b*) in fumarolic exhalations of the second scoria cone of the Great Tolbachik Fissure Eruption (Kamchatka peninsula, Russia). It belongs to a relatively rich family of sulfate–chloride minerals represented *e.g.* by kamchatkite KCu$_3$(SO$_4$)$_2$OCl, piypite K$_4$Cu$_4$O$_2$(SO$_4$)$_4$·(Na,Cu)Cl, chlorothionite K$_2$Cu(SO$_4$)Cl$_2$ and atlasovite Cu$^{2+}{}_6$Fe^{3+}Bi^{3+}O$_4$(SO$_4$)$_5$·KCl. The overwhelming majority of its members are copper-based species while there are just a handful of zinc sulfate minerals: hermannjahnite CuZn(SO$_4$)$_2$ (Siidra *et al.*, 2018*b*), glikinite Zn$_3$O(SO$_4$)$_2$ (Nazarchuk *et al.*, 2020) and majzlanite K$_2$Na(ZnNa)Ca(SO$_4$)$_4$ (Siidra *et al.*, 2020). Notably, belousovite is, to date, the only example of a natural anhydrous zinc sulfate halide.

The past decade has witnessed a series of illustrative examples when minerals proved to be archetypic not only for synthetic materials (Singh *et al.*, 2015; Kovrugin *et al.*, 2019; Borisov *et al.*, 2021) but also for numerous isostructural families (Siidra *et al.*, 2018*a*, 2021*a*). Examples are also rapidly accumulating when synthetic extension of these families results in rich polymorphism and/or morphotropism (Kálmán, 2005); some of these are reviewed by Siidra *et al.* (2022).

A synthetic analog of belousovite has been reported, along with two isostructural compounds $RbZn(SO_4)Cl$ and $TlZn(SO_4)Cl$, via melting $ACl + ZnSO_4$ mixtures at 550°C (Bosson, 1973, 1976). Gedam *et al.* (2006) attempted to prepare Ce^{3+}-, Dy^{3+}- and Mn^{n+}-doped $KZn(SO_4)Cl$ by room-temperature evaporation of aqueous solutions for photoluminescence studies. However, no crystallographic data had been reported, except for the PXRD data which were not interpreted, hence the chemical identity of the reported species remains obscure. From purely crystallographic considerations, structural analogs of belousovite [as well as other structures corresponding to the $AM(TO_4)X$ formula] are very likely to be found among compounds of other monovalent cations, including Na^+, Tl^+, NH_4^+ and Cs^+ and halides (bromides and iodides). The existence of selenate and even chromate analogs is less likely due to the high oxidizing potential of Se^{VI} and Cr^{VI}, yet examples are known when Se^{VI} and Cr^{VI} coexist with halide anions (Skakle *et al.*, 1996; Curda *et al.*, 2001; Siidra & Markovski, 2021). In addition, numerous examples are known where small molecular anions such as NO_3^- and SCN^- behave as analogs of halides so several test experiments were also conducted. There also exists a yet unresolved question of the identity of the formal magnesium analog of belousovite [anhydrokainite (Jänecke, 1912; Borisov *et al.*, 2022)]. Hence, we addressed the possibility of substituting Be^{2+}, Mg^{2+}, Co^{2+} and Cd^{2+} for Zn^{2+} in several test runs.

2. Experimental

2.1. Synthesis

Caution! The compounds of beryllium, selenium and particularly of thallium are highly toxic. Thallous halides are volatile ($p \simeq 10$ mmHg at the synthesis temperature). Such work can only be performed in a properly equipped laboratory by a trained personnel.

Two synthetic approaches were applied (Fig. 1). The first, chosen by analogy to the work of Bosson (1976), employed the melt technique. Alkali (Na–Cs, preheated at 150°C for 1–2 h) or thallous halide and anhydrous zinc sulfate (preheated at 450°C for 3–4 h) were taken in 1:1 molar ratio (2–3 mmol each), mixed, rapidly ground, placed into silica tubes and evacuated upon slow heating to 100–150°C (except the Tl-containing samples due to the high volatility of Tl*X*) until the residual pressure dropped to 2.5–3 $\times$ 10^{-2} mmHg, and then the silica tubes were flame sealed. The tubes (6 mm inner diameter, 150 mm long) were placed in a horizontal furnace so that the 'cold' end protruded slightly beyond the furnace to collect residues of water and other volatile species, heated to 525–550°C at a ramp of 50°C h^{-1}, soaked at this temperature for 48–60 h, and cooled to 300°C within 60 h, after which the furnace was switched off. In the samples containing NaBr, NaI, KI and TlI, essential amounts of crystalline sublimate condensed in the cold part of the tubes. The sublimates deliquesced rapidly in air and most likely corresponded to anhydrous ZnX_2. In these cases, no target compound was formed in the solidified melts. This method produced the majority of the alkali (thallous) zinc sulfate halides.

The test experiments performed with $MgSO_4$, $CdSO_4$ and $CoSO_4$ also did not result in belousovite analogs. Reaction of KCl and $CoSO_4$ produced high-quality dark blue and pink crystals of K_2CoCl_4 (Vermin *et al.*, 1976) and $K_2Co_2(SO_4)_3$

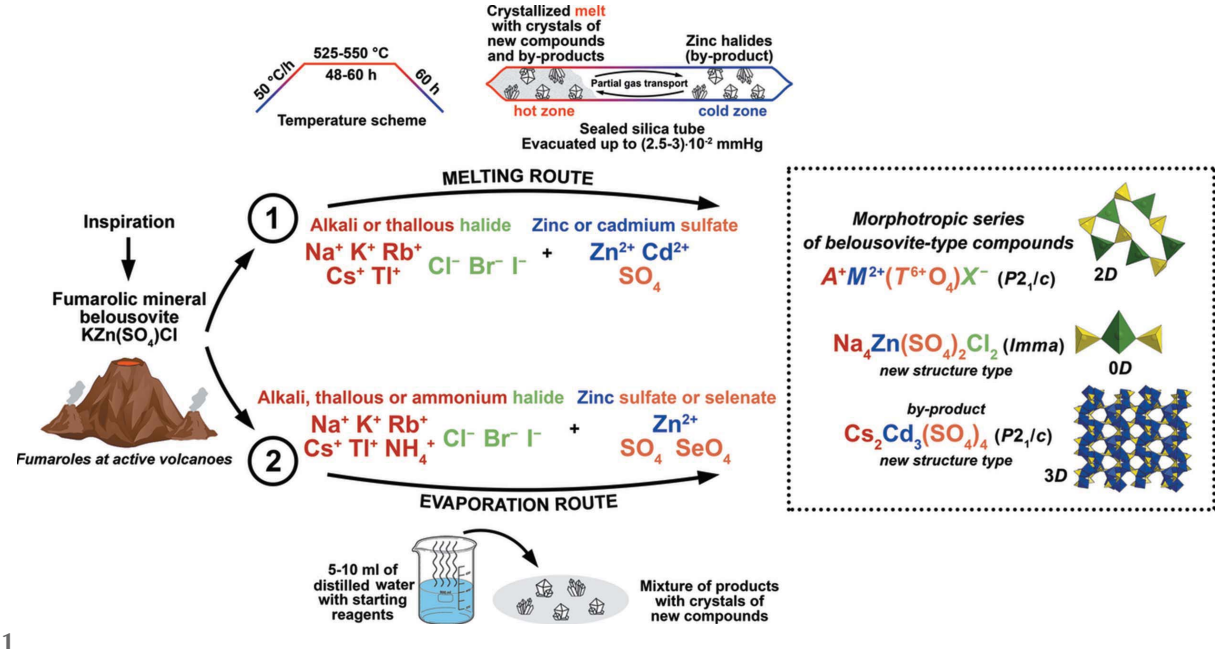

Figure 1
General strategy for the synthesis of belousovite-type compounds. See text for details.

(langbeinite) (Speer & Salje, 1986), respectively. Large, high-quality crystals of synthetic $K_2Mg_2(SO_4)_3$ langbeinite were also produced upon interaction of KCl and $MgSO_4$ at various temperatures. Reaction of CsCl and $CdSO_4$ did produce, however, a new sulfate species, $Cs_2Cd_3(SO_4)_4$ which is described below. No interaction was observed between caesium or rubidium chlorides and zinc chromate at 500–550°C. Use of higher temperatures led to partial reduction of Cr^{VI} to Cr^{III} with the formation of green by-products and pressure buildup.

A single experiment emulating natural conditions was performed for $KZn(SO_4)Cl$. A 1:1 mixture of KCl and $ZnSO_4{\cdot}7H_2O$ was ground, placed in a porcelain boat inside a silica reactor in a tubular furnace, and heated slowly to 550°C in a stream of air passed through a wash bottle charged with concentrated hydrochloric acid. According to PXRD data, the solidified melt was mainly $KZn(SO_4)Cl$ containing 3–5% of impurities.

The other synthetic approach (solution synthesis) was employed in preparation of compounds involving thermally unstable species, including ammonium salts and selenates. Zinc selenate was prepared by dissolving zinc hydroxide carbonate in *ca* 40% selenous acid. The solution was filtered and evaporated slowly at ambient conditions until dried. A mixture of alkali or ammonium halide and zinc sulfate heptahydrate or zinc selenate hexahydrate (1:1 molar ratio; 10 mmol each) was dissolved in distilled water (5–10 ml) and evaporated on a steam bath or heating plate until crystallization started and the amount of liquid phase dropped to ~1 ml. The crystals were rapidly separated using a small glass filter. Generally, the mother liquor solidified upon cooling, with the formation of various hydrates which were also analyzed. This method could not be applied to insoluble thallous halides. Attempts to dehydrate zinc selenate resulted in its reduction into some water insoluble white powder, most likely zinc selenite which was not further studied. This approach produced two new ammonium-bearing sulfate members, $NH_4Zn(SO_4)Cl$ and $NH_4Zn(SO_4)Br$, as well as the two selenate species, $RbZn(SeO_4)Br$ and $CsZn(SeO_4)Cl$. Test experiments also indicated that some belousovite species, including $KZn(SO_4)Cl$, can be produced via both solution and melt techniques.

A redox reaction started immediately upon contact of $ZnSeO_4$ and iodides. No new compound was found in test experiments with zinc sulfate and potassium nitrate or thiocyanate. When the solutions containing alkali or ammonium halide and zinc sulfate or selenate were left to evaporate at ambient conditions, crystals of Tutton salts, $A_2Zn(TO_4)_2{\cdot}6H_2O$, were invariably produced. These compounds were also abundant in the solidified mother liquors in the experiments described above, and most outcomes of selenate-based experiments. In a similar vein, a couple of runs were performed with solutions containing beryllium sulfate and sodium or potassium halides. New compounds were also not found in these experiments. It should be noted that both melt and solution techniques produced multiphase samples, and selection of the target crystals was in some cases a rather daunting task, since the crystal habits of belousovite analogs and Tutton salts (both colorless) are sometimes similar.

As a result of a series of syntheses described above, 14 belousovite-type compounds were obtained. Besides synthetic belousovite $KZn(SO_4)Cl$, its bromide analog $KZn(SO_4)Br$ was obtained. The compounds of the largest alkali cations Cs^+ and Rb^+ are formed with three different halogens (Cl, Br and I). Akin to K^+, NH_4^+ and Tl^+ contribute to chlorides and bromides only. Note that $RbZn(SO_4)Cl$ and $TlZn(SO_4)Cl$ have been studied previously (Bosson, 1973, 1976); their crystal structures are refined to higher precision in the present work. Among selenates, only $CsZn(SeO_4)Cl$ and $RbZn(SeO_4)Br$ were observed in the current study.

With the smaller Na^+ cation, a chemically and structurally different compound $Na_4Zn(SO_4)_2Cl_2$ was obtained instead of the expected $NaZn(SO_4)Cl$. Interaction of CsCl and $CdSO_4$ also yielded not the targeted belousovite analog but a novel binary sulfate, $Cs_2Cd_3(SO_4)_4$. These two compounds are also described below.

2.2. Single-crystal X-ray studies

The crystals of studied compounds were examined under an optical microscope and suitable ones selected and mounted on glass fibers for the data collection. The single-crystal X-ray experiments for all studied compounds (except NH_4-containing species) were carried out using a Bruker APEX-II CCD diffractometer with a micro-focus sealed X-ray tube (Mo $K\alpha$ radiation) operating at 50 kV and 0.6 mA. The data collection (at 296 K) and reduction procedures (integration, absorption correction, scaling and setting up initial *SHELX* files) were performed using the Bruker *APEX2* and Bruker *SAINT* (Bruker, 2014) program packages. All structures were solved using direct methods. The *SHELXT* and *SHELXL* program (Sheldrick, 2015) were used for the crystal structure solution and refinement, respectively. All experimental details are given in Tables 1, 2 and 3.

The data collections for $(NH_4)Zn(SO_4)Cl$ and $(NH_4)Zn(SO_4)Br$ were carried out using Rigaku Oxford Diffraction SuperNova and XtaLAB Synergy diffractometers, respectively, in a stream of cold (100 K) nitrogen gas. The use of low temperature suppresses rotation of the pseudo-spherical ammonium cation and enables the localization of weakly scattering hydrogen atoms and analysis of the patterns of hydrogen bonding. The data were integrated and corrected by means of the *CrysAlisPro* (Rigaku Oxford Diffraction, 2021) program package, which was also used to apply an empirical absorption correction using spherical harmonics, as implemented in the SCALE3 ABSPACK scaling algorithm. The structures of $AZn(SO_4)Cl$ with A = K, Rb and Tl were refined to obtain a single-source data set. Tables S1–S16 show the bond-valence sums for all structures calculated using parameters given by Gagné & Hawthorne (2015).

Table 1
Experimental details for sulfate belousovite-type compounds.

	$KZn(SO_4)Cl$	$KZn(SO_4)Br$	$NH_4Zn(SO_4)Cl$	$NH_4Zn(SO_4)Br$
Crystal data				
M_r	235.98	280.44	214.92	259.38
Crystal system, space group	Monoclinic, $P2_1/c$	Monoclinic, $P2_1/c$	Monoclinic, $P2_1/c$	Monoclinic, $P2_1/c$
Temperature (K)	296	296	100	100
a, b, c (Å)	6.9324 (16), 9.606 (2), 8.2227 (19)	7.0420 (5), 9.7207 (7), 8.4233 (6)	7.2019 (3), 9.5479 (4), 8.2214 (4)	7.3255 (2), 9.6732 (3), 8.5038 (3)
β (°)	96.524 (5)	98.201 (2)	95.107 (4)	97.505 (3)
V (Å^3)	544.0 (2)	570.71 (7)	563.08 (4)	597.43 (3)
Z	4	4	4	4
Radiation type	Mo $K\alpha$	Mo $K\alpha$	Mo $K\alpha$	Cu $K\alpha$
μ (mm^{-1})	6.07	12.32	5.13	16.37
Crystal size (mm)	0.04 × 0.03 × 0.03	0.02 × 0.02 × 0.01	0.07 × 0.05 × 0.04	0.06 × 0.04 × 0.03
Data collection				
Diffractometer	Bruker APEX-II CCD	Bruker APEX-II CCD	SuperNova, Dual, Atlas	XtaLAB Synergy, HyPix
Absorption correction	Multi-scan (*SAINT*)	Multi-scan (*SAINT*)	Multi-scan (*CrysAlis PRO*). Empirical absorption correction using spherical harmonics, implemented in SCALE3 ABSPACK scaling algorithm.	Multi-scan (*CrysAlis PRO*). Empirical absorption correction using spherical harmonics, implemented in SCALE3 ABSPACK scaling algorithm.
T_{min}, T_{max}	0.598, 0.745	0.523, 0.747	0.742, 1.000	0.689, 1.000
No. of measured, independent and observed [$I > 2\sigma(I)$] reflections	3581, 1060, 859	5382, 1369, 1155	2619, 1289, 1140	3475, 1201, 1076
R_{int}	0.029	0.036	0.061	0.026
(sin $\theta/\lambda)_{max}$ (Å^{-1})	0.632	0.661	0.659	0.631
Refinement				
$R[F^2 > 2\sigma(F^2)]$, $wR(F^2)$, S	0.028, 0.060, 1.02	0.025, 0.060, 1.08	0.041, 0.117, 1.05	0.026, 0.071, 1.09
No. of reflections	1060	1369	1289	1201
No. of parameters	73	74	89	89
No. of restraints	0	0	22	4
H-atom treatment	–	–	All H-atom parameters refined	All H-atom parameters refined
$\Delta\rho_{max}$, $\Delta\rho_{min}$ (e Å^{-3})	0.48, −0.55	0.54, −0.98	1.04, −1.25	0.64, −0.82

	$RbZn(SO_4)Br$	$RbZn(SO_4)Cl$	$RbZn(SO_4)I$	$TlZn(SO_4)Cl$
Crystal data				
M_r	326.81	282.35	373.80	401.25
Crystal system, space group	Monoclinic, $P2_1/c$	Monoclinic, $P2_1/c$	Monoclinic, $P2_1/c$	Monoclinic, $P2_1/c$
Temperature (K)	296	296	296	296
a, b, c (Å)	7.3573 (1), 9.7091 (2), 8.5753 (2)	7.2692 (5), 9.6261 (7), 8.3178 (6)	7.5036 (10), 9.8981 (13), 8.8015 (12)	7.341 (2), 9.622 (3), 8.1632 (16)
β (°)	97.820 (1)	95.524 (2)	99.175 (4)	94.012 (10)
V (Å^3)	606.86 (2)	579.33 (7)	645.34 (15)	575.2 (3)
Z	4	4	4	4
Radiation type	Mo $K\alpha$	Mo $K\alpha$	Mo $K\alpha$	Mo $K\alpha$
μ (mm^{-1})	18.87	13.33	16.33	32.90
Crystal size (mm)	0.03 × 0.02 × 0.02	0.04 × 0.02 × 0.01	0.06 × 0.04 × 0.03	0.04 × 0.04 × 0.02
Data collection				
Diffractometer	Bruker APEX-II CCD	Bruker APEX-II CCD	Bruker APEX-II CCD	Bruker APEX-II CCD
Absorption correction	Multi-scan (*SAINT*)	Multi-scan (*SAINT*)	Multi-scan (*SAINT*)	Multi-scan (*SAINT*)
T_{min}, T_{max}	0.530, 0.750	0.545, 0.747	0.584, 0.747	0.610, 0.747
No. of measured, independent and observed [$I > 2\sigma(I)$] reflections	7200, 1445, 1386	7838, 2304, 1805	9981, 2602, 1829	3675, 1362, 962
R_{int}	0.020	0.028	0.090	0.050
(sin $\theta/\lambda)_{max}$ (Å^{-1})	0.660	0.782	0.784	0.660
Refinement				
$R[F^2 > 2\sigma(F^2)]$, $wR(F^2)$, S	0.017, 0.039, 1.14	0.026, 0.057, 1.03	0.033, 0.063, 0.85	0.045, 0.077, 1.05
No. of reflections	1445	2304	2602	1362
No. of parameters	74	73	73	73
No. of restraints	0	0	0	0
H-atom treatment	–	–	–	–
$\Delta\rho_{max}$, $\Delta\rho_{min}$ (e Å^{-3})	0.66, −0.54	0.62, −0.58	1.81, −1.82	1.56, −1.17

	$TlZn(SO_4)Br$	$CsZn(SO_4)Cl$	$CsZn(SO_4)Br$	$CsZn(SO_4)I$
Crystal data				
M_r	445.71	329.79	374.25	421.24
Crystal system, space group	Monoclinic, $P2_1/c$	Monoclinic, $P2_1/c$	Monoclinic, $P2_1/c$	Monoclinic, $P2_1/c$
Temperature (K)	296	296	296	296
a, b, c (Å)	7.3746 (12), 9.7060 (16), 8.3810 (12)	7.6854 (5), 9.6794 (7), 8.4492 (6)	7.7892 (7), 9.791 (1), 8.7355 (8)	9.449 (3), 8.311 (2), 9.393 (2)
β (°)	96.370 (6)	95.303 (1)	97.290 (2)	96.982 (13)
V (Å^3)	596.19 (16)	625.85 (8)	660.82 (11)	732.2 (4)
Z	4	4	4	4
Radiation type	Mo $K\alpha$	Mo $K\alpha$	Mo $K\alpha$	Mo $K\alpha$
μ (mm^{-1})	37.99	10.34	15.44	12.69
Crystal size (mm)	0.06 × 0.05 × 0.03	0.08 × 0.06 × 0.03	0.05 × 0.04 × 0.03	0.06 × 0.04 × 0.03
Data collection				
Diffractometer	Bruker APEX-II CCD	Bruker APEX-II CCD	Bruker APEX-II CCD	Bruker APEX-II CCD
Absorption correction	Multi-scan (*SAINT*)	Multi-scan (*SAINT*)	Multi-scan (*SAINT*)	Multi-scan (*SAINT*)
T_{min}, T_{max}	0.626, 0.746	0.626, 0.747	0.645, 0.746	0.535, 0.748
No. of measured, independent and observed [$I > 2\sigma(I)$] reflections	10308, 1429, 1134	9324, 2704, 2000	7969, 2241, 1779	5357, 1742, 1517
R_{int}	0.065	0.033	0.025	0.031
$(\sin\theta/\lambda)_{max}$ (Å^{-1})	0.660	0.801	0.739	0.660
Refinement				
$R[F^2 > 2\sigma(F^2)]$, $wR(F^2)$, S	0.031, 0.051, 1.04	0.027, 0.054, 1.02	0.025, 0.044, 1.03	0.036, 0.093, 1.05
No. of reflections	1429	2704	2241	1742
No. of parameters	73	73	73	73
No. of restraints	0	0	0	0
H-atom treatment	–	–	–	–
$\Delta\rho_{max}$, $\Delta\rho_{min}$ (e Å^{-3})	0.88, −1.18	0.83, −1.11	0.80, −0.75	1.39, −1.69

Computer programs: *APEX2*, *SAINT* (Bruker, 2014), *CrysAlisPro* (1.171.41.104a, 1.171.41.86a; Rigaku Oxford Diffraction, 2021), *SHELXT-2018/2*, *SHELXL2018/3* (Sheldrick, 2015), *DIAMOND* (Brandenburg, 2020).

Table 2
Experimental details for selenate compounds.

	$CsZn(SeO_4)Cl$	$RbZn(SeO_4)Br$
M_r	376.69	373.71
Crystal system, space group	Monoclinic, $P2_1/c$	Monoclinic, $P2_1/c$
Temperature (K)	296	296
a, b, c (Å)	7.7918 (6), 9.8987 (8), 8.4422 (7)	7.461 (2), 9.998 (3), 8.703 (3)
β (°)	92.982 (3)	96.221 (8)
V (Å^3)	650.25 (9)	645.3 (3)
Z	4	4
Radiation type	Mo $K\alpha$	Mo $K\alpha$
μ (mm^{-1})	15.23	23.06
Crystal size (mm)	0.05 × 0.04 × 0.03	0.07 × 0.05 × 0.04
Data collection		
Diffractometer	Bruker APEX-II CCD	Bruker APEX-II CCD
Absorption correction	Multi-scan (*SAINT*)	Multi-scan (*SAINT*)
T_{min}, T_{max}	0.624, 0.746	0.403, 0.748
No. of measured, independent and observed [$I > 2\sigma(I)$] reflections	8627, 1563, 1261	16296, 1558, 1444
R_{int}	0.064	0.037
$(\sin\theta/\lambda)_{max}$ (Å^{-1})	0.660	0.660
Refinement		
$R[F^2 > 2\sigma(F^2)]$, $wR(F^2)$, S	0.036, 0.063, 1.04	0.018, 0.040, 1.12
No. of reflections	1563	1558
No. of parameters	73	74
$\Delta\rho_{max}$, $\Delta\rho_{min}$ (e Å^{-3})	0.90, −0.82	0.74, −0.54

Computer programs: *APEX2*, *SAINT* (Bruker, 2014), *SHELXT-2018/2*, *SHELXL2018/3* (Sheldrick, 2015), *DIAMOND* (Brandenburg, 2020).

2.3. Belousovite-type compounds $AZn(TO_4)X$ (A = K, Rb, Cs, Tl, NH_4; T = S, Se; X = Cl, Br, I)

Our studies have confirmed that the belousovite structure is archetypic for a relatively large family of isostructural synthetic compounds containing at least 12 sulfate and two selenate members. All these compounds adopt the same space group and the same set of Wyckoff sites, yet some structural and bonding details differ from one compound to another,

Table 3
Experimental details for $Na_4Zn(SO_4)_2Cl_2$ and $Cs_2Cd_3(SO_4)_4$.

	$Na_4Zn(SO_4)_2Cl_2$	$Cs_2Cd_3(SO_4)_4$
Crystal data		
M_r	210.18	1974.52
Crystal system, space group	Orthorhombic, *Imma*	Monoclinic, $P2_1/c$
Temperature (K)	296	296
a, b, c (Å)	10.4833 (10), 9.5543 (10), 10.2423 (10)	16.9563 (11), 9.3921 (6), 9.3799 (7)
α, β, γ (°)	90, 90, 90	90, 95.066 (2), 90
V (Å^3)	1025.87 (18)	1487.96 (18)
Z	8	2
Radiation type	Mo $K\alpha$	Mo $K\alpha$
μ (mm^{-1})	3.51	9.72
Crystal size (mm)	0.10 × 0.08 × 0.05	0.09 × 0.07 × 0.06
Data collection		
Diffractometer	Bruker APEX-II CCD	Bruker APEX-II CCD
Absorption correction	Multi-scan (*SAINT*)	Multi-scan (*SAINT*)
T_{min}, T_{max}	0.472, 0.746	0.653, 0.747
No. of measured, independent and observed [$I > 2\sigma(I)$] reflections	5180, 912, 706	25367, 6939, 5599
R_{int}	0.071	0.035
$(\sin\theta/\lambda)_{max}$ (Å^{-1})	0.743	0.824
Refinement		
$R[F^2 > 2\sigma(F^2)]$, $wR(F^2)$, S	0.030, 0.069, 0.94	0.026, 0.049, 1.04
No. of reflections	912	6939
No. of parameters	52	227
$\Delta\rho_{max}$, $\Delta\rho_{min}$ (e Å^{-3})	0.90, −0.60	1.52, −1.24

Computer programs: *APEX2*, *SAINT* (Bruker, 2014), *SHELXT-2018/2*, *SHELXL2018/3* (Sheldrick, 2015), *DIAMOND* (Brandenburg, 2020).

which are addressed below. There are unique sites for *A*, Zn, *T* and *X*. While *T* and Zn are tetrahedrally coordinated by 4O and 2O + 2*X*, respectively, the coordination of univalent cations exhibits essential variations.

2.3.1. Cation coordination. The coordination polyhedra of alkali and thallous cations are represented in Fig. 2. According to Brown (1981) all interactions giving more than 0.03 v.u. were taken into the consideration. The potassium cations in the structures of $KZn(SO_4)Cl$ and $KZn(SO_4)Br$ center the KO_5Cl_3 and KO_6Br_3 polyhedra, respectively; they are rather commonplace (Waroquiers *et al.*, 2017). As expected, the K–*X* (*X* = Cl, Br) distances are essentially longer compared to K–O with the mean values of 3.284 Å (K–Cl) and 3.431 Å (K–Br) against 2.872 Å and 2.960 Å for K–O separations. In the structure of $RbZn(SO_4)Cl$, Rb^+ adopts the RbO_6Cl_3 environment while in $RbZn(SO_4)Br$ the bond distances are somewhat different. Some Rb–O1 and Rb–Br separations are equal to 3.565 (2) and 3.5764 (4) Å. In $RbZn(SO_4)I$, the coordination number of Rb^+ increases and an RbO_6I_4 polyhedron is formed with ⟨Rb–O⟩ = 3.091 Å and ⟨Rb–I⟩ = 3.759 Å.

In sulfate chlorides, Tl^+ and Cs^+ adopt the same coordination within AO_6Cl_3 polyhedra. In their bromide analogs, Cs–O1 is essentially longer [3.792 (3) Å] than Tl–O1 [3.706 (5) Å]. The coordination of Cs^+ in the structure of $CsZn(SO_4)I$ is essentially different from the other cases and corresponds to a CsO_7I_2 polyhedron with ⟨Cs–O⟩ = 3.307 Å and ⟨Cs–I⟩ = 3.928 Å. In the two selenate analogs, the coordination of Cs^+ and Rb^+ can be described as CsO_6Cl_3 and RbO_5Br_3, which is again very common for these cations (Waroquiers *et al.*, 2017). In fact, replacement of SO_4^{2-} by slightly larger SeO_4^{2-} has a relatively small effect on the cation coordination.

The coordination of ammonium cations should be considered with regard to hydrogen bonding (Fig. 2, right). The interactions with separations of H···**A** < r(**A**) + 2 Å and <**D**H**A** (**D** = donor, **A** = acceptor) above 110° were taken into consideration (Steiner, 2002). The patterns of hydrogen bonding in the ammonium compounds are rather similar with the small differences probably caused by the anion radii. In the structure of the bromide, H1 forms a hydrogen bond to Br (which is not present in the structure of the chloride) with an H···Br separation of 2.99 (4) Å and ∠**D**H**A** = 115 (3)°. Compared to $NH_4Zn(SO_4)Cl$, in the structure of $(NH_4)Zn(SO_4)Br$ the ammonium group is slightly rotated relative to the sulfate tetrahedra, so that the H3···O1 separation increases to 2.65 Å, which is beyond the commonly accepted limit.

All structures of the belousovite-related sulfate compounds contain one symmetry-independent SO_4 group. The greatest distortion of the sulfate tetrahedron is observed for $NH_4Zn(SO_4)Cl$, where the mean ⟨S—O⟩ bond length is 1.457 Å, while the mean ⟨S—O⟩ bond length for sulfate minerals is 1.473 Å (Hawthorne *et al.*, 2000). This may reflect the stronger polarization induced by directed hydrogen bonds compared to symmetrical uniatomic cations. With the exception of $NH_4Zn(SO_4)Cl$, the average ⟨S—O⟩ value for the remaining structures is 1.471 Å. The distortion is also reflected in the volume of the polyhedra. The lowest value of 1.582 Å^3 is again characteristic for $NH_4Zn(SO_4)Cl$, while for the remaining structures the values of the sulfate tetrahedron

volume are in the range from 1.610 Å^3 for $CsZn(SO_4)Cl$ to 1.675 Å^3 for $TlZn(SO_4)Cl$.

The Zn cations center the ZnO_3X tetrahedra wherein all oxygen atoms are bridging and come from three distinct sulfate tetrahedra while the halide ligands are terminal. The Zn—X bond distances range from 2.1891 (10) Å in $(NH_4)Zn(SO_4)Cl$ to 2.5148 (5) Å in $RbZn(SO_4)I$, which is expectedly essentially above those for Zn—O [ranging from 1.939 (4) Å for Zn—O1 in $TlZn(SO_4)Br$ to 1.999 (3) Å in Zn–O2 in $RbZn(SO_4)I$]. Earlier, we noted (Siidra *et al.*, 2018*c*) that the ZnO_3Cl tetrahedron is observed most commonly among cases of mixed-ligand zinc coordination. Besides belousovite and its analogs, it is also present in the structures of minerals simonkolleite $Zn_5(OH)_8Cl_2{\cdot}H_2O$ (Hawthorne & Sokolova, 2002), chubarovite $KZn_2(BO_3)Cl_2$ (Pekov *et al.*, 2015) and gordaite $NaZn_4(SO_4)(OH)_6Cl{\cdot}6H_2O$ (Zhu *et al.*, 1997), as well as in two synthetic compounds, $CaZn_8(SO_4)_2(OH)_{12}Cl_2(H_2O)_9$ (Burns *et al.*, 1998) and $BaZn(TeO_3)Cl_2$ (Jiang *et al.*, 2006).

The selenate analogs of belousovite – $CsZn(SeO_4)Cl$ and $RbZn(SeO_4)Br$ – have a similar structural motif to sulfate structures. Changes of bond lengths in the studied selenates are caused by the larger size of the SeO_4^{2-} tetrahedron with a volume of 2.232 Å^3 and an average bond length of 1.635 Å.

2.3.2. Structure description. The structure of belousovite and its analogs is built of layers parallel to *bc* [Figs. 3(*a*)–3(*c*)] comprised of vertex-sharing ZnO_3X polyhedra [X = Cl, Br, I; Fig. 3(*d*)] linked by the sulfate (selenate) polyhedra to form $ZnXO_2(TO_4)$ 'building blocks' [Fig. 3(*e*)]. These layers contain four-membered rings with alternating '...up–down...' orientation of ZnO_3X and SO_4, as well as larger eight-membered rings [Fig. 3(*d*)]. The latter are of particular interest for monitoring the structural evolution and deformations with variation of chemical composition (mainly the nature of A and X). Earlier, we noted that the topology of the $Zn(TO_4)X$ frameworks are very close to that of apophyllite group minerals (Siidra *et al.*, 2018*c*; Liebau, 1985) with the only

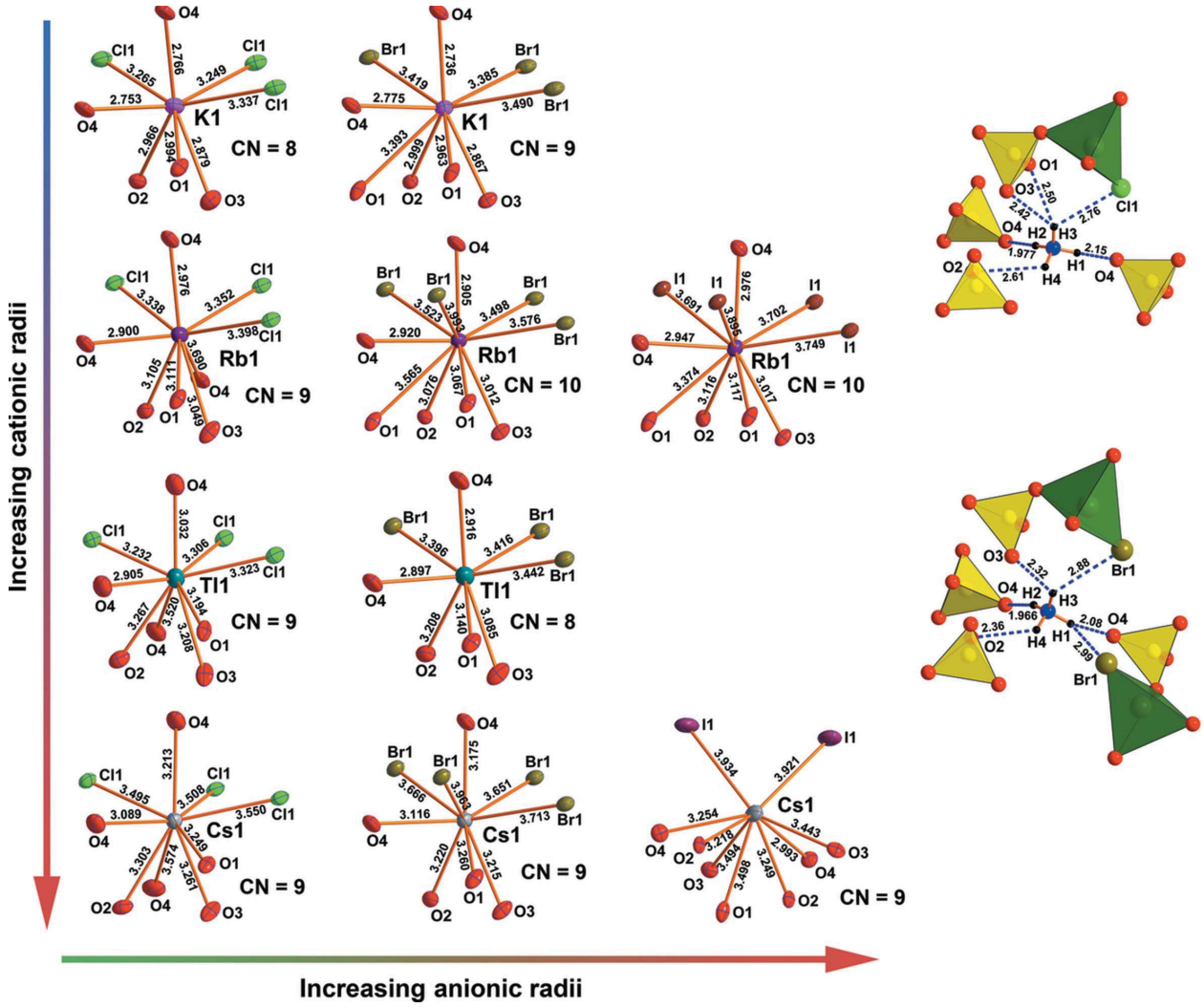

Figure 2
Left: coordination of the alkali and thallous cations in the sulfate analogs of belousovite. All polyhedra, except that in $CsZn(SO_4)I$, are given in nearly the same orientation, to facilitate comparison. Anisotropic displacement parameter ellipsoids are drawn at the 50% probability level. All interatomic distances are given in Å. Right: coordination of the ammonium cations in the structures of $(NH_4)Zn(SO_4)Cl$ (upper) and $(NH_4)Zn(SO_4)Br$ (lower).

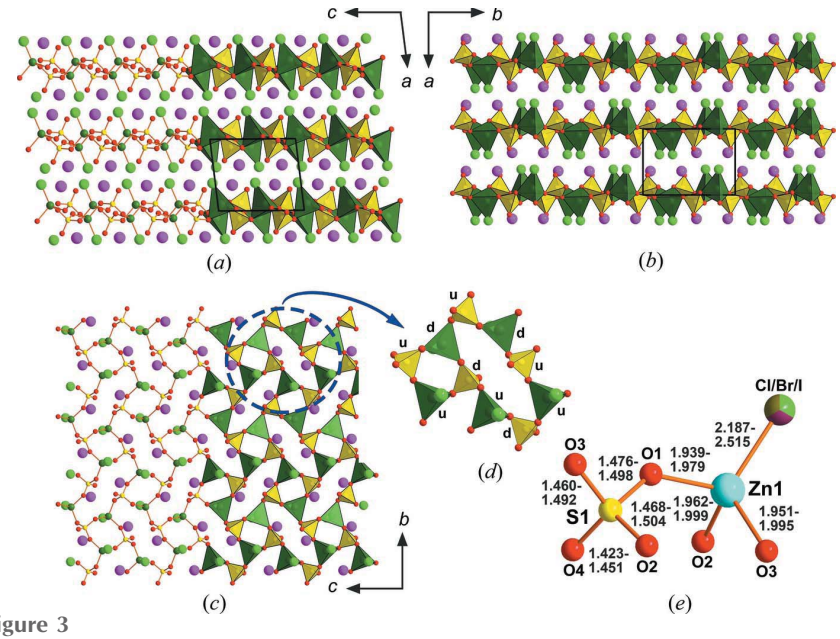

Figure 3
The crystal structure of $KZn(SO_4)Cl$ as the archetypic representative of its structure type, in ball-and-stick and polyhedral representation (*a*, *b*). A typical layer (*c*) formed by the four- and eight-membered rings (*d*). The mixed-ligand coordination of Zn and coordination of S with minimal and maximal bond distances (*e*). Distances are given in Å.

essential difference being that in the latter case, all tetrahedra of the four-membered rings have the same orientation.

The structure of $CsZn(SO_4)I$, containing the largest univalent cation and halide anion, exhibits the largest deviations from the common motif. As follows in Fig. 4, the anionic layers are noticeably stretched along *a*, with Zn–O–S bridges acting as hinges [Figs. 4(*a*)–4(*c*)]. The corrugation angle (φ) of the layers, measured at Zn atoms in a plane perpendicular to the corrugation, changes from 144.0° for $CsZn(SO_4)Br$ to 94.9° for $CsZn(SO_4)I$ [Figs. 4(*d*)–4(*f*)]. The separation between planes containing Zn atoms (which are aligned along *c*) increases to 3.20 Å from the minimal value of 1.32 Å for $KZn(SO_4)Cl$. This enables the structure of $CsZn(SO_4)I$ to be considered as a unique representative of a new morphotropic form in the $AZn(TO_4)X$ series.

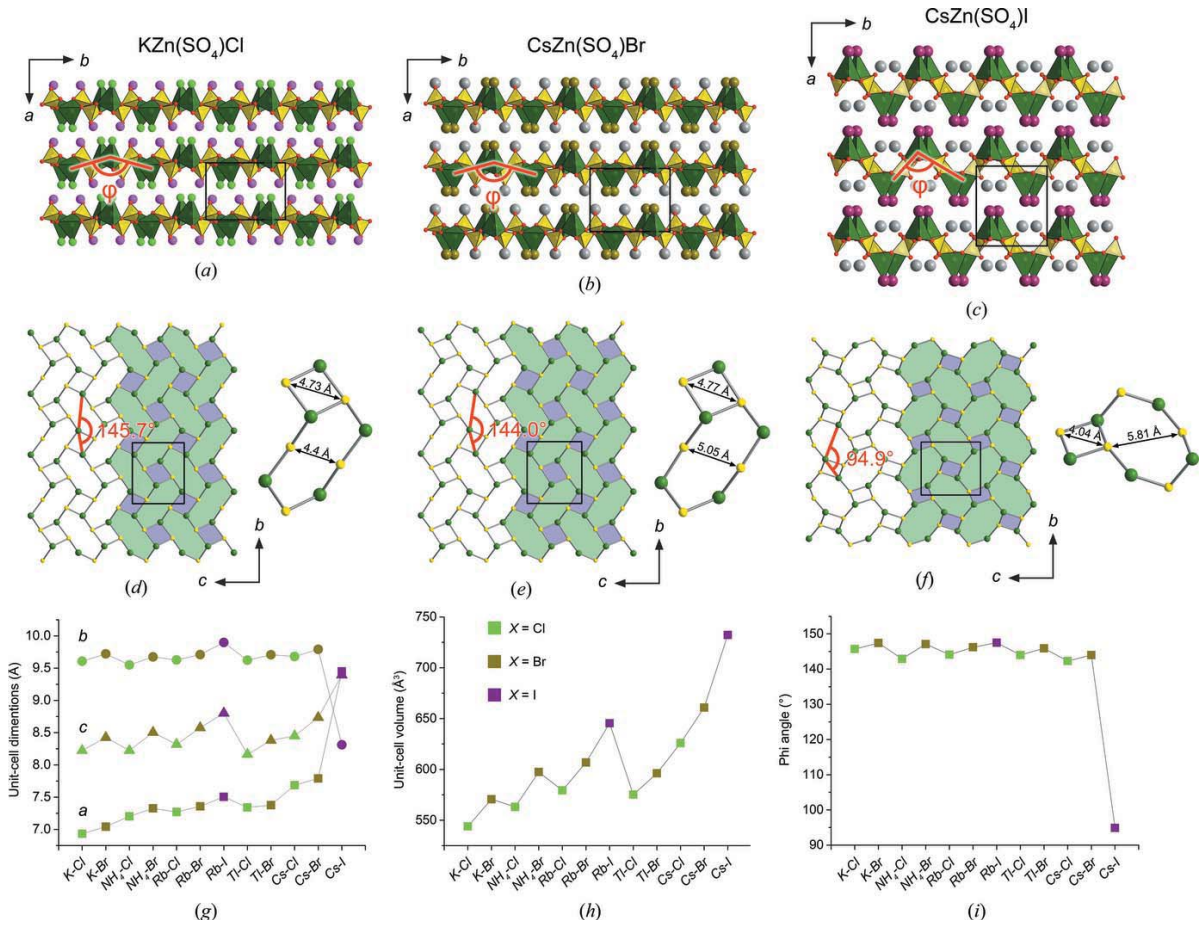

Figure 4
The crystal structures of $KZn(SO_4)Cl$ (*a*), $CsZn(SO_4)Br$ (*b*) and $CsZn(SO_4)I$ (*c*), showing maximum layer corrugation. From $KZn(SO_4)Cl$ to $CsZn(SO_4)Br$, the φ angle varies slightly (*d*,*e*), but decreases sharply to 94.9° in the case of $CsZn(SO_4)I$ (*f*). Graphs for the unit-cell dimension (*g*), volume (*h*) and φ angle (*i*) in studied belousovite-type structures.

2.4. $Na_4Zn(SO_4)_2Cl_2$

In contrast to its heavier alkali analogs, sodium does not contribute to the belousovite family. Instead, a new compound $Na_4Zn(SO_4)_2Cl_2$ is formed which represents a new structure type. This arrangement contains one site for Zn, S and Cl, and three symmetry-independent sites for Na and O. The zinc atom is tetrahedrally coordinated by two Cl atoms at 2.2437 (9) Å and two O1 atoms at 1.980 (2) Å, which correspond to two sulfate anions [Fig. 5(*a*)]. As expected, the S—O1 distance to the bridging oxygen atom is longer [1.501 (2) Å] than the terminal S—O2 [1.4718 (17) Å] and S—O3 [1.465 (2) Å] distances. The latter are closer to the mean value for sulfates (1.473 Å; Hawthorne *et al.*, 2000). Overall, the structure of $Na_4Zn(SO_4)_2Cl_2$ can be regarded as comprised of molecular $[ZnCl_2(SO_4)_2]^{4-}$ anions [Fig. 4(*a*)], aligned in the *ab* plane [Fig. 5(*b*)]. The remaining space is filled by the 'net' of three symmetry-independent sodium sites [Fig. 5(*c*)]. The latter is comprised of layers (parallel to *ab*) formed by Na1 and Na2, which alternate with Na3 along *c*. The Na1 and Na3 atoms are coordinated by four oxygen [*d*(Na—O) = 2.3393 (16)–2.4828 (19) Å] and two chlorine atoms [*d*(Na—Cl) 2.7185 (3) and 3.3261 (9) Å for Na1 and Na3, respectively] to center *trans*-NaO_4Cl_2 octahedra. Na2 is octahedrally coordinated by oxygen atoms only at ⟨Na2—O⟩ = 2.466 Å. The formation of ZnO_2X_2 oxyhalide tetrahedra is less common, yet observed in a series of natural and synthetic zinc selenite and tellurite halides (Semenova *et al.*, 1992; Johnsson & Törnroos, 2003*a*,*b*, 2007; Zhang & Johnsson, 2008). Note that in all these cases, except $CuZn(TeO_3)Cl_2$ (Johnsson & Törnroos, 2003*b*), zinc is present in several different oxyhalide coordinations, not only as ZnO_2X_2 tetrahedra. Also, attempts to prepare crystals of $CuZn(TeO_3)Br_2$ were not successful (Johnsson & Törnroos, 2003*b*), similar to our unsuccessful attempts to prepare $Na_4Zn(SO_4)_2Br_2$.

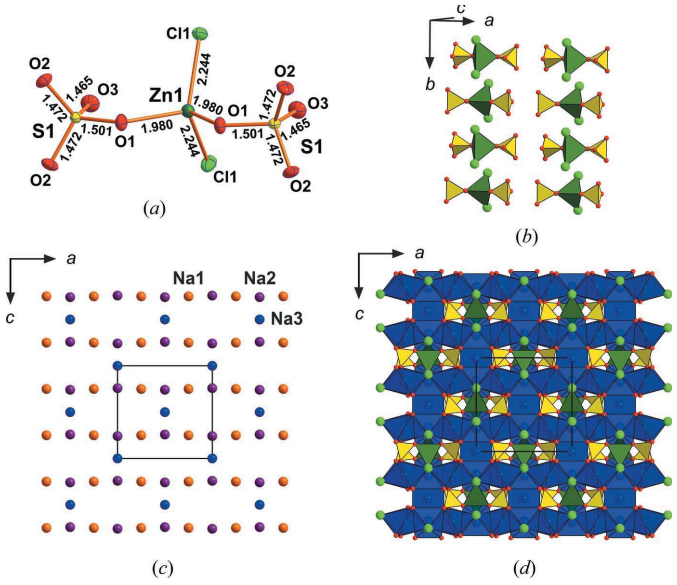

Figure 5
The 0D $[ZnCl_2(SO_4)_2]^{4-}$ anions in the structure of $Na_4Zn(SO_4)_2Cl_2$ (*a*) and their alignment along *ab* (*b*); the cationic sublattice (*c*) and overall structure of $Na_4Zn(SO_4)_2Cl_2$ (*d*).

2.5. $Cs_2Cd_3(SO_4)_4$

The crystal structure of the monoclinic by-product $Cs_2Cd_3(SO_4)_4$ also belongs to a new structure type and contains two Cs, three Cd and four S sites [Fig. 6(*a*)]. All Cd^{2+} cations are octahedrally coordinated by oxygen atoms which is quite common (Waroquiers *et al.*, 2017) with mean bond distances of 2.320, 2.311 and 2.269 Å for Cd1, Cd2 and Cd3, respectively. The sulfate tetrahedra are characterized by mean bond distances of 1.466 Å to 1.473 Å, which again correlates well to the reference values (Hawthorne *et al.*, 2000). The Cs1 and Cs2 sites exhibit as high coordination numbers as 11 and 13, respectively; the corresponding polyhedra are linked by sulfate groups [Fig. 6(*a*)]. The new structure can be regarded as a framework comprised of $[Cd_3(SO_4)_4]^{2-}$ blocks which can be deconvoluted into layers [Figs. 6(*b*)–6(*d*)]. The layers are comprised of Cd_2O_{10} dimers of edge-sharing $Cd1O_6$ and $Cd2O_6$ octahedra, tied additionally by the $S1O_4$ groups via O5 and O12. The $Cd3O_6$ octahedra are attached to these species via $S2O_4$ and $S3O_4$ tetrahedra adding up to the $[Cd_3(SO_4)_4]^{2-}$ blocks and forming the porous framework filled by Cs1 and Cs2 alternating along *a*.

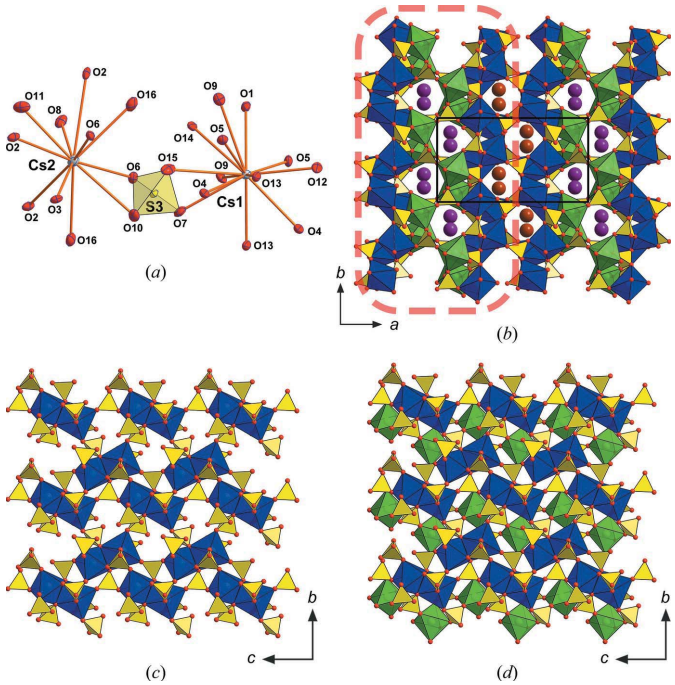

Figure 6
Coordination of Cs atoms in the crystal structure of $Cs_2Cd_3(SO_4)_4$ (*a*). General projection of the crystal structure of $Cs_2Cd_3(SO_4)_4$ (*b*). Designations: $Cd1O_6$, $Cd2O_6$ = blue; $Cd3O_6$ octahedra = blue; SO_4 = yellow; Cs1 atoms = brown balls; Cs2 atoms = violet balls. Framework of the structure of $Cs_2Cd_3(SO_4)_4$ consists of blocks (highlighted by the red dashed line) which can be split into layers. The layers are formed by Cd_2O_{10} dimeric units sharing common corners with SO_4 tetrahedra (*c*) and single CdO_6 octahedra inserted in the voids (*d*).

3. Discussion

Akin to a variety of minerals, belousovite also proved to be a predecessor for a relatively rich family of synthetic analogs. The structure is relatively flexible and able to accommodate univalent cations and halide anions of variable size (Fig. 4). It needs be noted, however, that the largest anion, I^-, can only be incorporated with the largest cations like Rb^+ and Cs^+, and the structure of $CsZn(SO_4)I$ differs rather from those of other members. Single crystals of only two selenate analogs could be prepared which is but too few to draw any reasonable conclusions. The formation of competitive Tutton salts in solution syntheses was observed in almost all cases but crystals of sulfate belousovites were more easy to produce in contrast to selenates which suggests that the latter are, in general, less stable. No representative had been observed with CrO_4^{2-}; this suggests that the belousovite structure is probably rather sensitive to the size of the tetrahedral oxyanions.

It also proved impossible to substitute Zn^{2+} by a variety of divalent cations of similar (Co^{2+}, Mg^{2+}), smaller (Be^{2+}) and larger (Cd^{2+}) size. While tetrahedral coordination is the most common for Be^{2+}, its coordination sphere is rather rigid and less prone to ligand exchange in aqueous solutions; note also the relatively large mismatch in the Lewis acid strength of Be^{2+} (L_a = 0.50) and basicity of sulfate (L_b = 0.17) and 'heavier' halide (L_b = 0.10–0.06) anions; relatively stable complexes are formed only with F^- (L_b = 0.21) (Brown, 1981). To the best of our knowledge, mixed BeO_nX_{4-n} (X = Cl, Br, I) coordination is either unknown or exceptionally rare. In contrast, Zn^{2+}, Mg^{2+} and Co^{2+} have nearly the same L_a values of 0.36–0.40 (Brown, 1981) which is closer to the L_b values of sulfate and heavier halides; Cd^{2+} (L_a = 0.32) is even softer (Gagné & Hawthorne, 2017). However, Cd^{2+}, Co^{2+} and Mg^{2+} more readily adopt an octahedral environment; mixed-ligand tetrahedral MO_3X and MO_2X_2 coordinations are unknown for Mg^{2+} and rather uncommon for Co^{2+} and Cd^{2+} [note the octahedral coordination of Cd^{2+} in $Cs_2Cd_2(SO_4)_3$].

The structure of $AZn(SO_4)X$ with X = Cl, Br, I differs from those of $AM(SO_4)F$ which have been reported for a variety of transition and non-transition M^{2+} cations (Barpanda *et al.*, 2011; Melot *et al.*, 2011; Reynaud *et al.*, 2012; Tripathi *et al.*, 2013; Lander *et al.*, 2015; Sun *et al.*, 2016; Ge *et al.*, 2018). Notably, in all these structures the M^{2+} cation adopts a mixed oxyfluoride octahedral coordination; in addition, these structures have been reported for the smaller univalent cations (Li^+, Na^+, K^+ and NH_4^+); larger ones (Tl^+, Rb^+ and Cs^+) are either not tolerated or have not been addressed. Hence, the $AM(SO_4)X$ family provides yet another example of morphotropism, a rather common phenomenon for anhydrous sulfates which we had addressed recently for $A_2Cu(SO_4)_2$ and $A_2M_2(SO_4)_3$ compositions (Siidra *et al.*, 2021*b*, 2022). Among fluoride sulfates, the prime structure-driving factor is probably the size of the alkali cation; in contrast, the belousovite architecture demonstrates a striking flexibility adopting a variety of cations and anions of quite different sizes.

The hitherto only anhydrous alkali zinc sulfate halide beyond the belousovite family, $Na_4Zn(SO_4)_2Cl_2$, exhibits totally different composition and unrelated structure. In this case, it was not possible to substitute Na^+ or Cl^- by their analogs. It would be interesting to see, given the abundance of sodium in the fumarolic exhalations, if a mineral analog of this compound could eventually be discovered.

The last compound to be addressed is the $Cs_2Cd_3(SO_4)_4$ double sulfate which also represents a new structure type. Despite the almost equal ionic radii of Cd^{2+} and Ca^{2+} (Shannon, 1976), it is not isostructural to $Cs_2Ca_3(SO_4)_4$ (Fang *et al.*, 2022). This stoichiometry $A^+_2M^{2+}_3(SO_4)_4$ was first identified for anhydrous sulfates in itelmenite $Na_2Cu_2Mg(SO_4)_4$ (Nazarchuk *et al.*, 2018), as well as in its recently described synthetic analogs (Nekrasova *et al.*, 2021). Other mineral-inspired representatives of this family may exist which requires extensive work in inorganic synthesis.

Acknowledgements

This work was performed within the task No. 0081-2022-0002. Technical support by the SPbSU X-ray Diffraction and Geomodel Resource Centers is gratefully acknowledged.

References

Ati, M., Melot, B. C., Chotard, J.-N., Rousse, G., Reynaud, M. & Tarascon, J.-M. (2011). *Electrochem. Commun.* **13**, 1280–1283.
Barpanda, P., Chotard, J.-N., Delacourt, C., Reynaud, M., Filinchuk, Y., Armand, M., Deschamps, M. & Tarascon, J.-M. (2011). *Angew. Chem. Int. Ed.* **50**, 2526–2531.
Borisov, A. S., Siidra, O. I., Kovrugin, V. M., Golov, A. A., Depmeier, W., Nazarchuk, E. V. & Holzheid, A. (2021). *J. Appl. Cryst.* **54**, 237–250.
Borisov, A. S., Siidra, O. I., Ugolkov, V. L., Kuznetsov, A. N., Firsova, V. A., Charkin, D. O., Platonova, N. V. & Pekov, I. V. (2022). *Mineral. Mag.* **86**, 37–48.
Bosson, B. (1973). *Acta Chem. Scand.* **27**, 2230–2231.
Bosson, B. (1976). *Acta Cryst.* B**32**, 2044–2047.
Brandenburg, K. (2020). *DIAMOND*. Crystal Impact GbR, Bonn, Germany.
Brown, I. D. (1981). In *Structure and Bonding in Crystals*, Vol. 2, edited by M. O'Keeffe and A. Navrotsky, pp. 1–30. New York: Academic Press.
Bruker (2014). *APEX2* and *SAINT*. Bruker-AXS Inc., Madison, Wisconsin, USA.
Burns, P. C., Roberts, A. C. & Nikischer, A. J. (1998). *Eur. J. Mineral.* **10**, 923–930.
Curda, J., Peters, E. M., Klein, W. & Jansen, M. (2001). *Z. Kristallogr. New Cryst. Struct.* **216**, 190.
Fang, P., Tang, W., Shen, Y., Hong, J., Li, Y. & Jia, J. (2022). *Crystals*, **12**, 126.
Fujihala, M., Mitsuda, S., Mole, R. A., Yu, D. H., Watanabe, I., Yano, S., Kuwai, T., Sagayama, H., Kouchi, T., Kamebuchi, H. & Tadokoro, M. (2020*a*). *Phys. Rev. B*, **101**, 024410.
Fujihala, M., Morita, K., Mole, R., Mitsuda, S., Tohyama, T., Yano, S., Yu, D., Sota, S., Kuwai, Y., Koda, A., Okabe, H., Lee, H., Itoh, S., Hawai, T., Masuda, T., Sagayama, A., Matsuo, A., Kindo, K., Ohira-Kawamura, S. & Nakajima, K. (2020*b*). *Nat. Commun.* **11**, 3429.
Gagné, O. C. & Hawthorne, F. C. (2015). *Acta Cryst.* B**71**, 562–578.
Gagné, O. C. & Hawthorne, F. C. (2017). *Acta Cryst.* B**73**, 956–961.
Ge, G., Luo, W., Zhang, L., Du, X. & Liang, L. (2018). *Polyhedron*, **152**, 55–60.
Gedam, S. C., Dhoble, S. J. & Moharil, S. V. (2006). *J. Lumin.* **121**, 450–455.
Hälg, M., Lorenz, W. E. A., Povarov, K. Yu., Månsson, M., Skourski, Y. & Zheludev, A. (2014). *Phys. Rev. B*, **90**, 174413.

Hawthorne, F. C., Krivovichev, S. V. & Burns, P. C. (2000). *Rev. Mineral. Geochem.* **40**, 1–112.
Hawthorne, F. C. & Sokolova, E. (2002). *Can. Mineral.* **40**, 939–946.
Jänecke, E. (1912). *Z. Phys. Chem.* **80U**, 1–12.
Jiang, H., Feng, M. L. & Mao, J. G. (2006). *J. Solid State Chem.* **179**, 1911–1917.
Johnsson, M. & Törnroos, K. W. (2003*a*). *Acta Cryst.* C**59**, i53–i54.
Johnsson, M. & Törnroos, K. W. (2003*b*). *Solid State Sci.* **5**, 263–266.
Johnsson, M. & Törnroos, K. W. (2007). *Acta Cryst.* C**63**, i34–i36.
Kálmán, A. (2005). *Acta Cryst.* B**61**, 536–547.
Kikuchi, H., Kunieda, K., Fujii, Y., Astuti, F., Sari, D. P. & Watanabe, I. (2017). *RIKEN Accel. Prog. Rep.* **50**, 236.
Kovrugin, V. M., Nekrasova, D. O., Siidra, O. I., Mentré, O., Masquelier, C., Stefanovich, S. Yu. & Colmont, M. (2019). *Cryst. Growth Des.* **19**, 1233–1244.
Lander, L., Rousse, G., Abakumov, A. M., Sougrati, M., van Tendeloo, G. & Tarascon, J.-M. (2015). *J. Mater. Chem. A*, **3**, 19754–19764.
Liebau, F. (1985). *Structural Chemistry of Silicates. Structure, Bonding and Classification*. Berlin, Heidelberg, New York, Tokyo: Springer.
Melot, B. C., Rousse, G., Chotard, J.-N., Ati, M., Rodríguez-Carvajal, J., Kemei, M. C. & Tarascon, J.-M. (2011). *Chem. Mater.* **23**, 2922–2930.
Nazarchuk, E. V., Siidra, O. I., Agakhanov, A. A., Lukina, E. A., Avdontseva, E. Yu. & Karpov, G. A. (2018). *Mineral. Mag.* **82**, 1233–1241.
Nazarchuk, E. V., Siidra, O. I., Nekrasova, D. O., Shilovskikh, V. V., Borisov, A. S. & Avdontseva, E. Yu. (2020). *Mineral. Mag.* **84**, 563–567.
Nekrasova, D. O., Siidra, O. I., Zaitsev, A. N., Ugolkov, V. L., Colmont, M., Charkin, D. O., Mentré, O., Chen, R., Kovrugin, V. M. & Borisov, A. S. (2021). *Phys. Chem. Miner.* **48**, 6.
Pekov, I. V., Zubkova, N. V., Pautov, L. A., Yapaskurt, V. O., Chukanov, N. V., Lykova, I. S., Britvin, S. N., Sidorov, E. G. & Pushcharovsky, D. Y. (2015). *Can. Mineral.* **53**, 273–284.
Reynaud, M., Barpanda, P., Rousse, G., Chotard, J.-N., Melot, D. B., Recham, N. & Tarascon, J.-M. (2012). *Solid State Sci.* **14**, 15–20.
Rigaku Oxford Diffraction (2021). *CrysAlisPro*. Rigaku Oxford Diffraction, Oxford, UK.
Semenova, T. F., Rozhdestvenskaya, I. V., Filatov, S. K. & Vergasova, L. P. (1992). *Mineral. Mag.* **56**, 241–245.
Shannon, R. D. (1976). *Acta Cryst.* A**32**, 751–767.
Sheldrick, G. M. (2015). *Acta Cryst.* C**71**, 3–8.
Siidra, O., Nekrasova, D., Blatova, O., Colmont, M., Mentre, O. & Charkin, D. (2022). *Acta Cryst.* B**78**, 153–161.
Siidra, O. I., Charkin, D., Kovrugin, V. M. & Borisov, A. S. (2021*a*). *Acta Cryst.* B**77**, 1003–1011.
Siidra, O. I., Lukina, E. A., Nazarchuk, E. V., Depmeier, W., Bubnova, R. S., Agakhanov, A. A., Avdontseva, E. Yu., Filatov, S. K. & Kovrugin, V. M. (2018*a*). *Mineral. Mag.* **82**, 257–274.
Siidra, O. I. & Markovski, M. R. (2021). *Z. Kristallogr.* **236**, 173–178.
Siidra, O. I., Nazarchuk, E. V., Agakhanov, A. A., Lukina, E. A., Zaitsev, A. N., Turner, R., Filatov, S. K., Pekov, I. V., Karpov, G. A. & Yapaskurt, V. O. (2018*b*). *Mineral. Petrol.* **112**, 123–134.
Siidra, O. I., Nazarchuk, E. V., Lukina, E. A., Zaitsev, A. N. & Shilovskikh, V. V. (2018*c*). *Mineral. Mag.* **82**, 1079–1088.
Siidra, O. I., Nazarchuk, E. V., Zaitsev, A. N. & Shilovskikh, V. V. (2020). *Mineral. Mag.* **84**, 153–158.
Siidra, O. I., Nekrasova, D. O., Charkin, D. O., Zaitsev, A. N., Borisov, A. S., Colmont, M., Mentré, O. & Spiridonova, D. V. (2021*b*). *Mineral. Mag.* **85**, 831–845.
Singh, P., Shiva, K., Celio, H. & Goodenough, J. B. (2015). *Energy Environ. Sci.* **8**, 3000–3005.
Skakle, J. M. S., Fletcher, J. G. & West, A. R. (1996). *An. Quim.-Int.* **92**, 358–361.
Soldatov, T. A., Smirnov, A. I., Povarov, K. Yu., Hälg, M., Lorenz, W. E. A. & Zheludev, A. (2018). *Phys. Rev. B*, **98**, 144440.
Speer, D. & Salje, E. (1986). *Phys. Chem. Miner.* **13**, 17–24.
Steiner, T. (2002). *Angew. Chem. Int. Ed.* **41**, 48–76.
Sun, M., Rousse, G., Corte, D. D., Saubanère, M., Doublet, M.-L. & Tarascon, J.-M. (2016). *Chem. Mater.* **28**, 1607–1610.
Tripathi, R., Popov, G., Sun, X., Ryan, D. H. & Nazar, L. F. (2013). *J. Mater. Chem. A*, **1**, 2990–2994.
Vergasova, L. P. & Filatov, S. K. (2016). *J. Volcanol. Seismol.* **10**, 71–85.
Vermin, W. J., Verschoor, G. C. & Ijdo, D. J. W. (1976). *Acta Cryst.* B**32**, 3325–3328.
Waroquiers, D., Gonze, X., Rignanese, G.-M., Welker-Nieuwoudt, C., Rosowski, F., Göbel, M., Schenk, S., Degelmann, P., André, R., Glaum, R. & Hautier, G. (2017). *Chem. Mater.* **29**, 8346–8360.
Zhang, D. & Johnsson, M. (2008). *Acta Cryst.* E**64**, i26.
Zhu, L., Seff, K., Witzke, T. & Nasdala, L. (1997). *J. Chem. Crystallogr.* **27**, 325–329.